Supporting information

Fabrication of cartilage-inspired hydrogel/entangled polymer-elastomer structures possessing poroelastic properties

Siavash Soltanahmadi[a], Nicholas Raske[b], Gregory N de Boer[a], Anne Neville[a], Robert W Hewson[b], Michael G Bryant[a*]

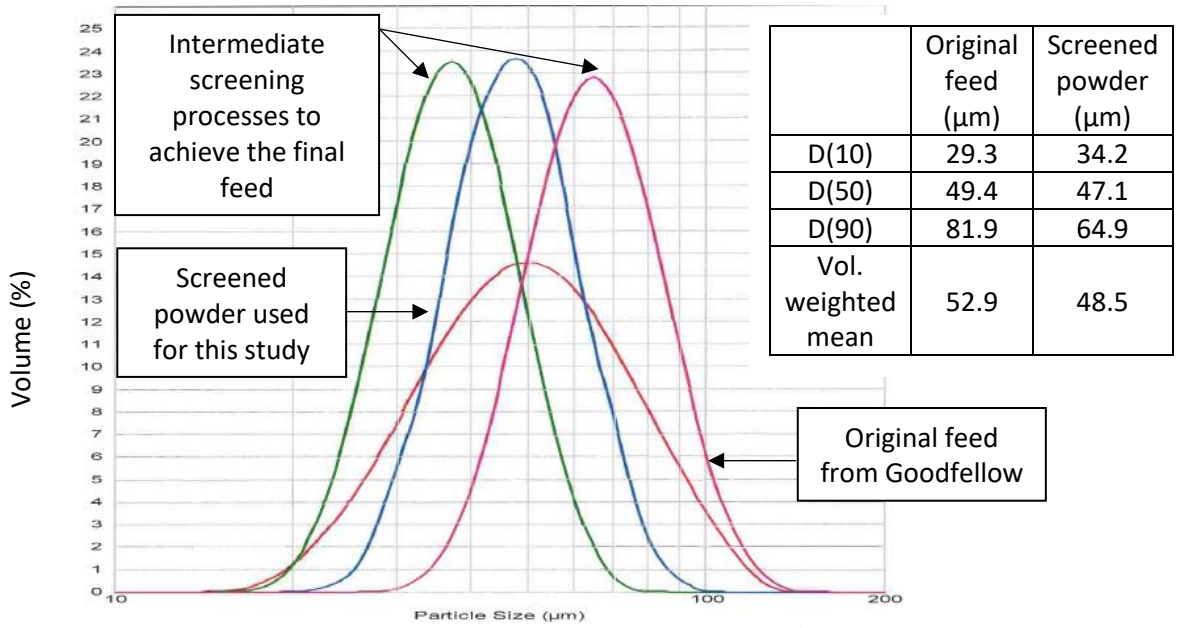
*M.G.Bryant@leeds.ac.uk

[a] School of Mechanical Engineering, University of Leeds, Leeds, LS2 9JT, UK

[b] Department of Aeronautics, Imperial College London, London, SW7 2AZ, UK

Size distribution of PMMA particles

Un-crosslinked polymethylmethacrylate spherical particles were purchased from Goodfellow. A Scirocco 2000 Air Jet classifier (Hosokawa Micron LTD) was used to achieve a tighter particle size distribution whilst maintaining a D50 (i.e. median diameter, D stands for diameter of particles and D50 is a volume-based size distribution parameter indicating the size point below which a cumulative 50% of the powder is contained) close to 45-50µm. The sieving results are shown in Figure S 1.



	Original feed (µm)	Screened powder (µm)
D(10)	29.3	34.2
D(50)	49.4	47.1
D(90)	81.9	64.9
Vol. weighted mean	52.9	48.5

Figure S 1. Size distribution histograms of the original and classified/sieved particles and associated D parameters

For this study, a topping and tailing procedure was performed where fine and coarse fractions of particles from either end of the powder were removed. The efficiency of the procedure was assessed by size distribution analysis using a Malvern Mastersizer instrument and an Aerosil additive as an anti-static agent to reduce cohesive forces between particles. Histograms of particle size distribution for the original feed (i.e. unprocessed purchased powder; red curve) and the screened powder (i.e. air jet sieved powder used to fabricate the PDMS sponge; blue curve) are shown in Figure S 1. The screened powder had a narrower size distribution when compared to the feed powder. The screened powder,

used for this study, had a median diameter of around 47 µm and a volume weighted mean diameter (i.e. D(4,3)) of around 48 µm.

UV/Vis analysis of the dense PDMS and PDMS sponge

Discs of 25 mm diameter and 2 mm thick were prepared from the dense PDMS and PDMS sponge. A UV-Vis-NIR spectrophotometer was used to obtain transmittance spectra for the wavelengths ranging from 190 to 800 nm (Figure S 2). As expected for the dense PDMS, intense absorption peaks were observed in wavelengths below 300 nm. The UV lamp used in this study emitted an UV wavelength range of 300-400 nm. The dense PDMS was, therefore, transparent to the UV wavelength range irradiated by the lamp. The PDMS sponge showed a spectrum with absorption peaks within a similar wavelength range to the dense PDMS. However, a 30-40% decrease in transmittance of the incident UV illumination was observed for the PDMS sponge. This suggests that the irradiation intensity changes as a function of the material depth and can be fractionally lower deeper into the material.

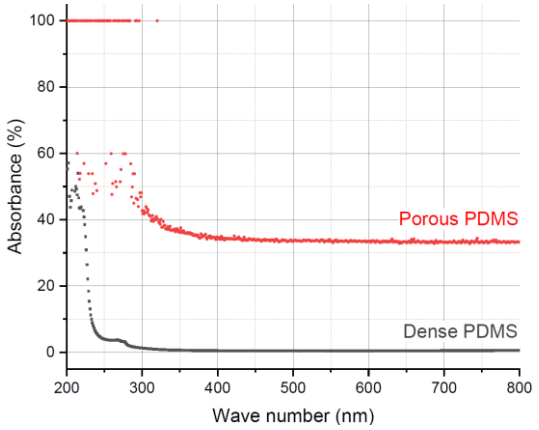


Figure S 2. UV-Vis spectra of the dense and porous PDMS

The setup for permeability measurement

The developed cell to measure permeability of materials is shown in Figure 5. The cell was embedded in a setup comprising a syringe pump (Cole-Parmer 74900), integrated with a glass syringe (Eterna Matic Sanitex, EM304, 30 ml), and a manometer (Digitron P200M). The setup is shown in Figure S 3(a). Nylon tubes and pneumatic fittings were used to connect the cell to the other components. For each material three separate samples were prepared. The differential pressure between the inlet and outlet of the cell was measured at three flow rates as shown in Figure S 3(b). The line of regression of the differential pressure data on the flow rate data for each sample was determined to calculate permeability of the sample. The slope of the line was used to solve the Darcy's law of permeability for each sample. The permeability of each material, reported in Figure 5, is an average of the permeability values of three samples.

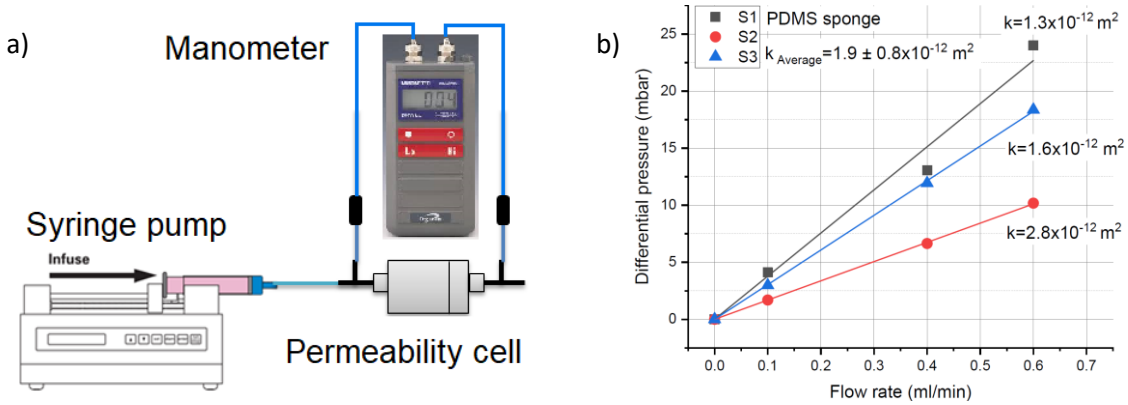


Figure S 3. a) illustration of the setup for permeability measurement and b) linear regression of the differential pressure data at three flow rates for the PDMS sponge

Cyclic compression tests

In order to examine the recovery of load-bearing behaviour of materials, 10-cycle compression experiments were carried out using the Mecmesin instrument with a pause phase of 15 s. Following

on from the 1st loading cycle, the next consecutive cycles instigated immediately from the absolute zero position where the flat porous indenter was fully retracted to a zero load condition and the tare loading was conducted for each cycle. The cyclic compression results for the gel-PDMS and the PDMS sponge with all cycles starting from the absolute zero position are shown in Figure S 4. The dissipated energy and load-recovery within each cycle are summarised with the figure insets. As can be seen in Figure S 4, all the cyclic graphs were almost identical for the gel-PDMS and the PDMS sponge at both strain rates. For the gel-PDMS compressed at 0.83 s^{-1}, the reduction in the energy dissipation at the second cycle was negligible (~1%). The energy dissipation throughout all cycles always remained above 96% of its initial value for the gel-PDMS at 0.83 s^{-1}. The reduction in the energy dissipation within cyclic tests from the tare load (Figure 7) was 24-26%. The trivial reduction in the energy dissipation within cyclic tests from the absolute zero position together with a less than 2% reduction in the peak-load recovery (compared to 5% reduction within tests from the tare load) showed that the gel-PDMS composite immediately recovered to almost its initial properties once the load was fully retracted to a zero load position. At 16x10^{-3} s^{-1}, the decay of load-bearing properties of the gel-PDMS material was minor and very similar to cyclic tests from the tare load (Figure 7). The peak-load recovery for cycles between 2 and 10 was higher than 100% (i.e. the peak-load in the 2nd cycle onwards was greater than that in the 1st cycle) and a maximum reduction of 12% was observed in the energy dissipation. For the PDMS sponge, the peak-load recovery between cycle 2 and 10 was discerned to remain beyond 98% at both strain rates. A slight reduction in the dissipated energy (4-15%) compared to the first cycle was observed for cycles 2 to 10.

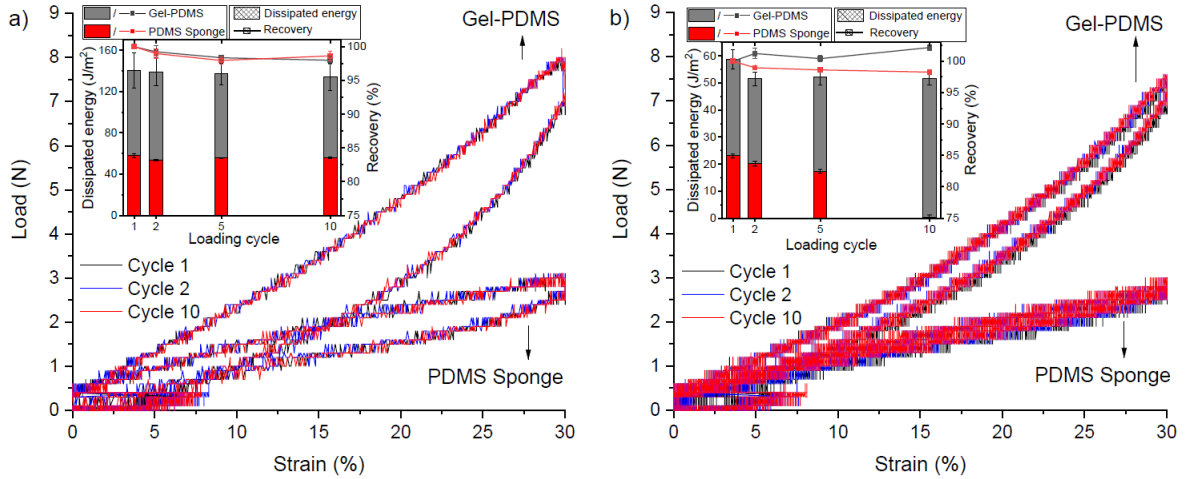


Figure S 4. Load-strain curves for cyclic compression testing of the gel-PDMS and PDMS sponge (dry-PDMS condition) materials to a strain limit of 30% with a 15-second pause phase included in between the loading and unloading phases at strain rates of a) 0.83 s^{-1} and b) 16x10^{-3} s^{-1}. Graphs for cycles 1,2 and 10 only are presented for clarity since there was no noticeable difference between cycles 2 to 10. The 2nd to 10th cycles consecutively started from the absolute zero position immediately following the full retraction of the flat porous indenter to a zero load position. The inset in the graph shows the dissipated energy during each cycle (column) and the peak-load recovery (ratio of the peak-load at each cycle to the peak-load at the first cycle which is presented by symbol-line).

The setup for compression tests

As shown in Figure S 5(a), the set-up developed for compression testing comprised a flat porous indenter, a flat porous drainage plate, a cylindrical water bath and a metallic indenter holder. The porous indenter and drainage were made from PMMA particles with a mean particle size of 600 microns. The discs were sintered for 90 minutes at 180˚C (Figure S 5(b)). The 600 µm particles ensure a greater permeability of the indenter and drainage as compared to the PDMS sponge. As can be seen

in Figure S 5(c), the PDMS sponge and resultant composites were impermeable on the cylindrical surface along the length which was sealed through a 50-100um thick PDMS layer during moulding processes.

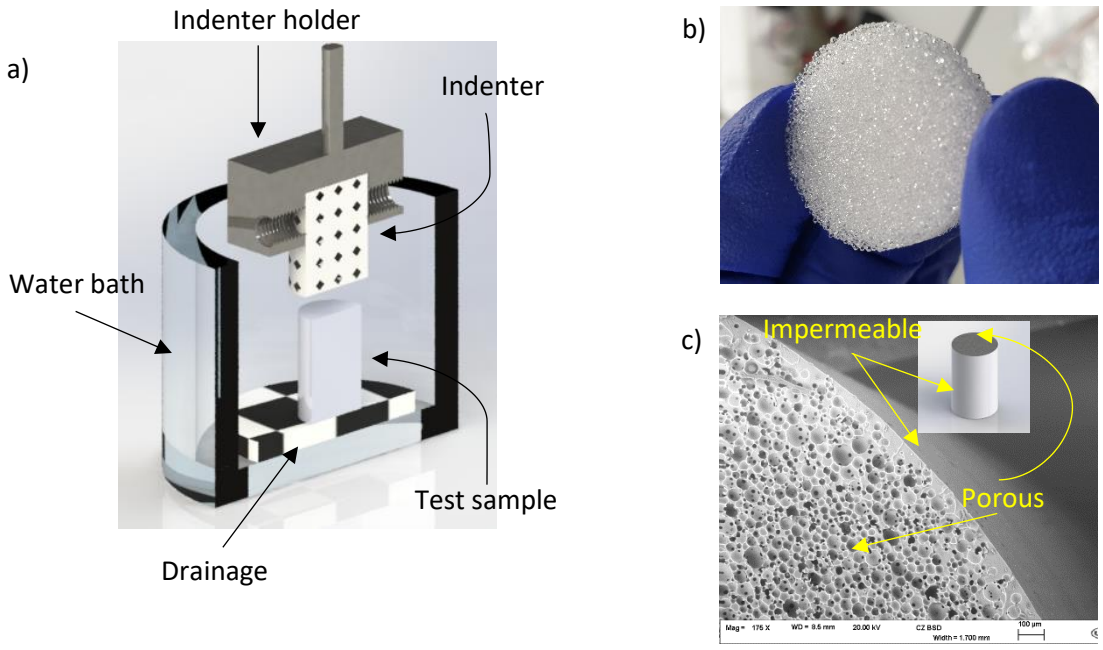


Figure S 5. a) illustration of a cross-section of the setup for compression tests, b) image of the porous drainage and c) SEM image of the PDMS sponge

ATR-FTIR analysis to confirm the complete dissolution of the PMMA template

ATR-FTIR was used to confirm the complete removal of the PMMA particles to reveal the PDMS sponge with no residual traces of the PMMA within its matrix. Shown in Figure S 6, small traces of the residual PMMA prompted a peak at around 1721 cm^{-1} which has been attributed to the C=O bond in PMMA. This peak is a characteristic peak for PMMA and cannot overlap with absorptions peaks from PDMS. All the PDMS sponge materials were analysed by ATR-FTIR to verify PMMA removal prior to any further analysis.

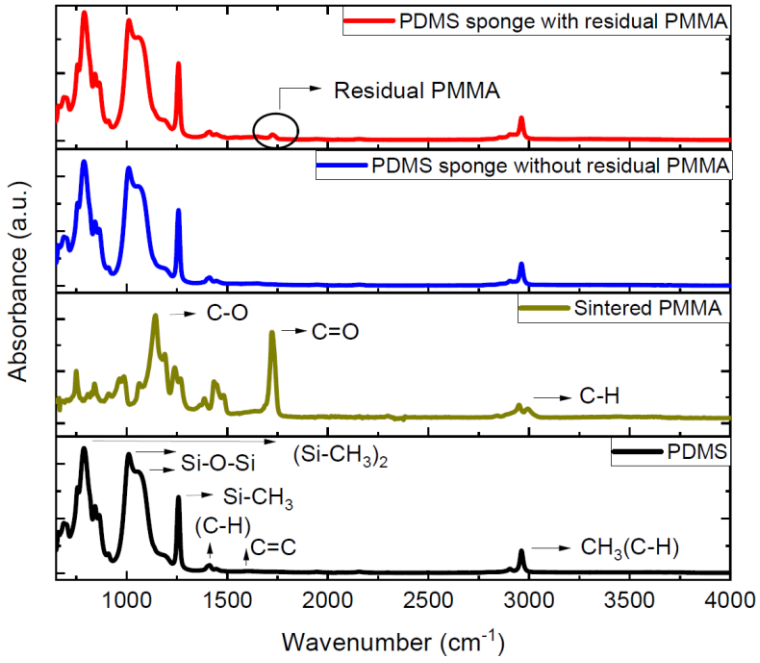


Figure S 6. ATR-FTIR spectra of the PDMS sponge with and without residual traces of PMMA, the sintered PMMA template and the reference PDMS

X-ray elemental mapping of the PDMS sponge

Energy Dispersive X-ray (EDX) spectroscopy was conducted on the cryo-sectioned silanised PDMS sponge to demonstrate the spherical porosity of the sponge. The cryo-SEM image and corresponding EDX elemental maps of the image are shown in Figure S 7 showing the spherical porosity. The higher contrast water-filled porous regions are visible in the cryo-SEM image. The K_α line of oxygen (presented in green) showed a higher intensity in the porous regions which arose from oxygen in water. The Si k_α signal (presented in red) was detected in the areas correlating with the PDMS material.

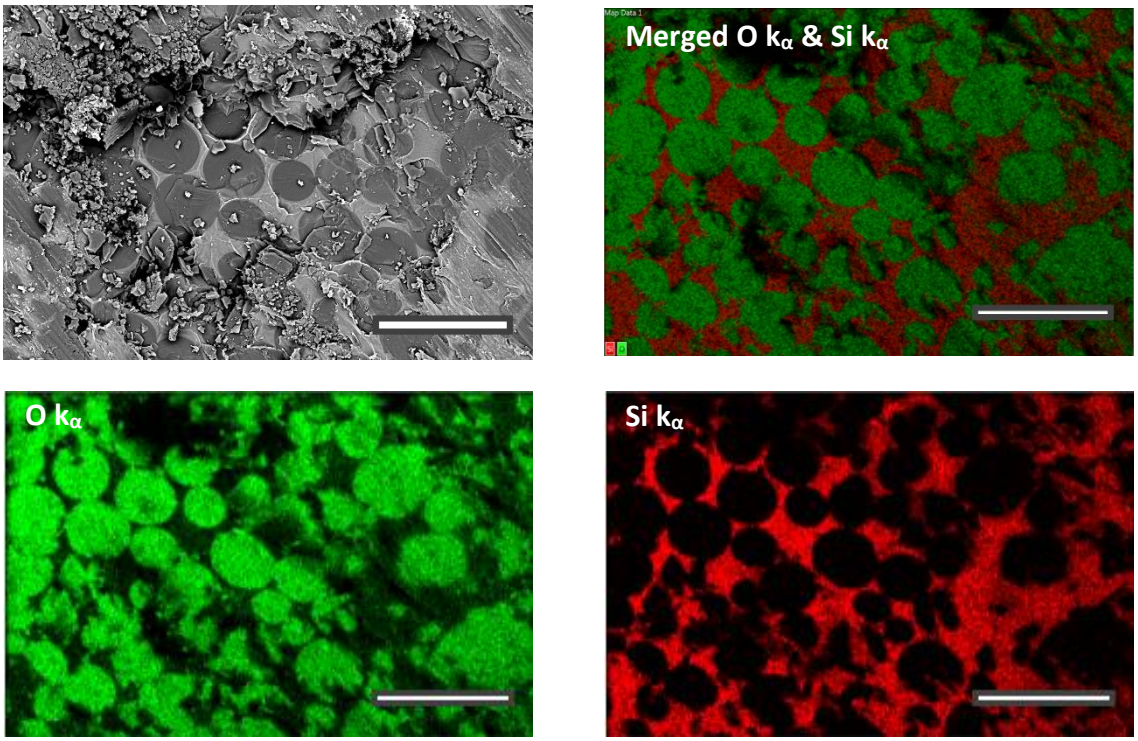


Figure S 7. A cryo-SEM image of the silanised PDMS sponge with the corresponding EDX elemental maps. The scale bar represents 100µm in the image and maps.

Fabrication of porous PDMS

PMMA particles were casted into glass-bottomed cylindrical stainless-steel moulds which were 16mm in length and had a bore diameter of 6.35mm. In order to induce open porosity in the sponge, PMMA particles were heat-sintered in an atmospheric oven at 180˚C (above its glass transition temperature) for 90 minutes. The sintering process facilitated viscous diffusion of PMMA chains in the particles into the neighbouring particles. This created a multi-directional interconnectivities between pores. The sintered particles were backfilled with PDMS elastomer (a blend of monomer and curing agent with a mass ratio of 10:1 respectively) under vacuum over a course of several hours. Special measures were taken to ensure that all gaps between PMMA particles were filled with PDMS. The PDMS infused PMMA template was cured at 100˚C over a 30-minute

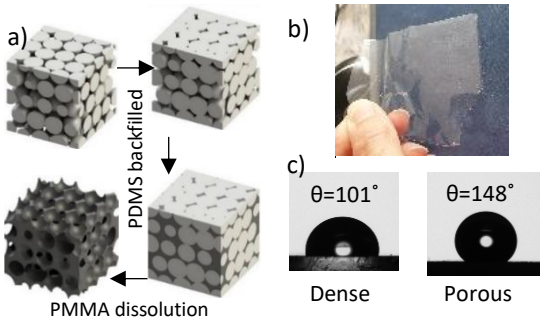


Figure S 8. a) fabrication method for the PDMS sponge, b) a PMMA film following the solvent extraction and C) WCA measurements of the dense and porous PDMS

period using an atmospheric oven. The composite of PDMS and PMMA particles was milled to 10mm length from both circular bases. At the final step, the composite was soaked in a good solvent for PMMA which can simultaneously swell PDMS (ethyl acetate in this case) and sonicated for 6 hours until PMMA particles were fully dissolved to reveal a porous PDMS elastomer. This methodology is shown in Figure S 8(a). The procedure is sustainable as the PMMA particles can be retrieved by solvent extraction. A PMMA film following the solvent extraction is presented in Figure S 8(b). Water contact angle measurements were carried out to assess the influence of porous texture characteristics of the PDMS sponge on wettability of materials. As can be seen in Figure S 8(c), the porous texture enhanced hydrophobicity of the PDMS by 47˚ to 148˚ which shows almost super-hydrophobic behaviour of the PDMS sponge.

Cry-SEM image form a pristine PDMS sponge

Figure S 9 presents a cryo-image from a water filled PDMS sponge evidencing the absence of silanised layer at the interface of pore surface and water in the pore.

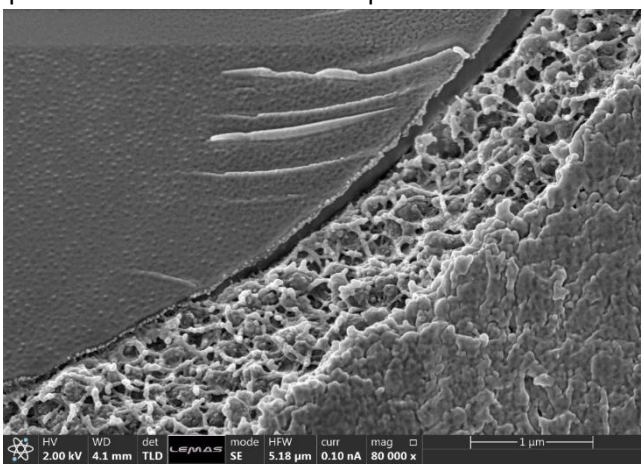


Figure S 9. A cryo-image from water filled PDMS sponge evidencing the absence of silanised layer at the interface of pore surface-water.

Structural similarities between cartilage and the gel-PDMS composite

Articular cartilage (excluding cellular matrix) primarily consists of three components water, collagen and proteoglycans[1]. Three-dimensional collagen fibrils provides solid (elastic) load bearing property and facilitate structural stability for proteoglycan which retain water within the structure (poroelasticity).

Figure S 10(a) shows an electron micrograph from collagen fibrillar structure of cartilage surface following removal of the non-calcified cartilage. The circle in the image is 55 microns and shows a diameter equivalent to that of an average fibre bundle[1] which is similar in size as compared to the main pores in the PDMS-sponge (40-60 micron) shown in Figure S 10(b). Comparing Figure S 10(c) with Figure S 10(d) showing collagen fibres of human hyaline cartilage[2] and microstructure of PDMS respectively, it appears that the pores in PDMS crosslinked network and the network of collagen fibers are in similar size scales (100 nm - 1 um). Figure S 10(e) presents the PAAm crosslinked network within the pores in PDMS-sponge which has similar function to proteoglycans in cartilage retaining water within the structure and imparting poroelastic behaviour.

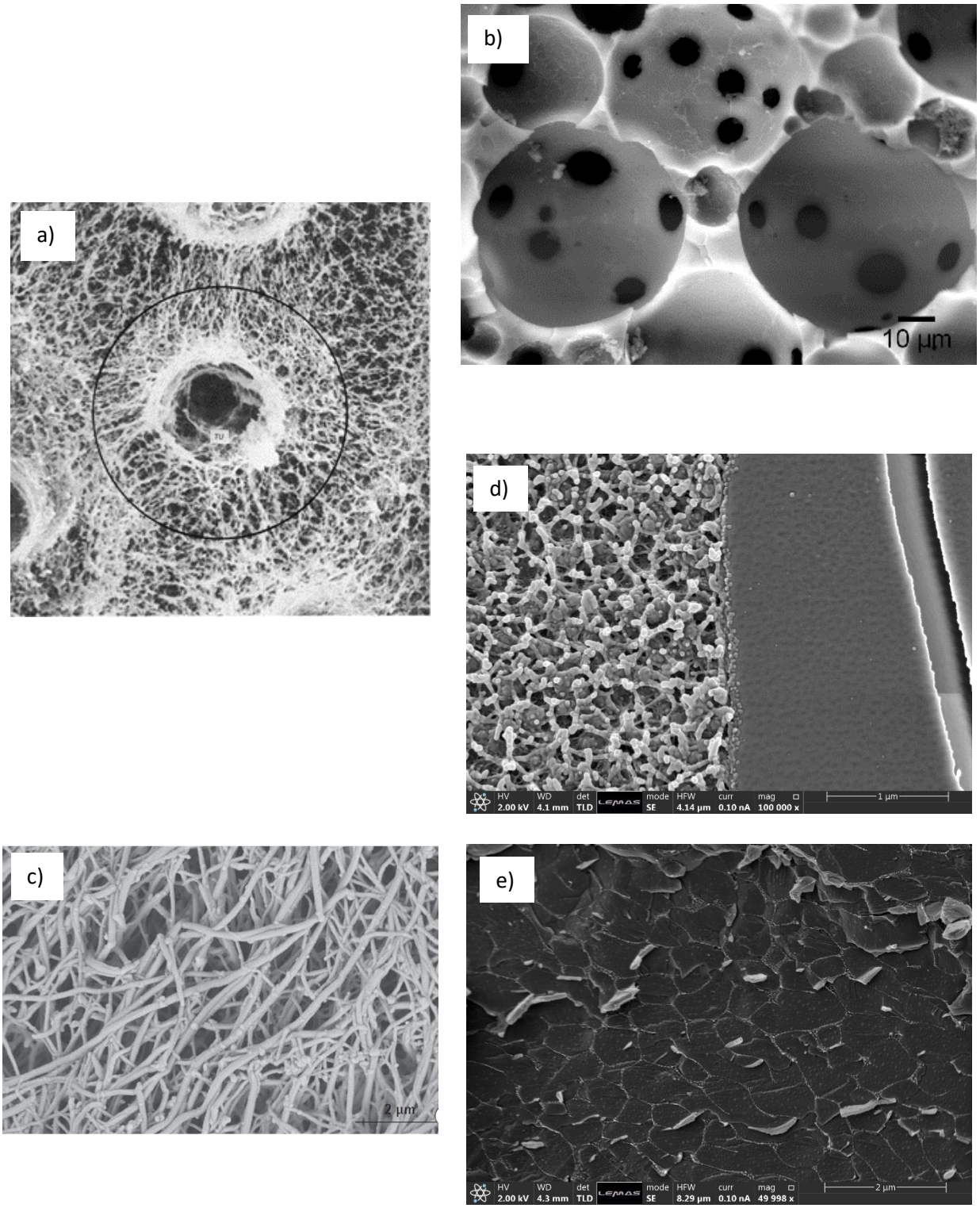


Figure S 10. Electron micrographs from a) cartilage after removal of un-calcified collagen fibrils[1], b) PDMS sponge, c) extracellular matrix and collagen fibres of human hyaline cartilage [2], d) microstructure of PDMS network and e) PAAm hydrogel grafted into the pores of PDMS sponge.

Swelling tests

In order to examine the influence water exposure on swelling of the gel-PDMS, the sample was soaked in DI water and the dimensions and sample weights were measured after gel grafting and following 48 hr/14 days of water immersion. The results show negligible changes to the dimensions.

Table S 1. Water immersions tests. The influence swelling on dimensional change of the gel-PDMS sample was assessed over a span of two weeks at room temperature. (n=3x5)

Time	Before PAAm grafting	As-produced (gel-grafted)	48 hr	14 days
Diameter (mm)	6.32 ± 0.02	6.38 ± 0.04	6.37 ± 0.05	6.39 ± 0.06
Length (mm)	9.9 ± 0.25	10.1 ± 0.1	10.1 ± 0.1	-
Weight (mg)	152 ± 34	317 ± 47	324 ± 53	333 ± 47

Cyclic compression tests

In order to further examine the recovery of load-bearing behaviour of materials, 100-cycle compression experiments were carried out using the Mecmesin instrument with no pause phase (shown in Figure S 11). Following on from the 1st loading cycle, the next consecutive cycles instigated immediately from the tare-loading position. For the gel-PDMS compressed at 0.83 s^{-1} at the 10th cycle a 4% reduction in the peak-load was observed. A notable difference either in the energy dissipation or the peak-load recovery was not found for cycles between 10 and 100. The peak-load recovery stayed above 95% and energy dissipation remained above 78% for these cycles. This confirms the promising load-recovery behaviour of the gel-PDMS at higher number of cycles (100) under the testing conditions defined in this study.

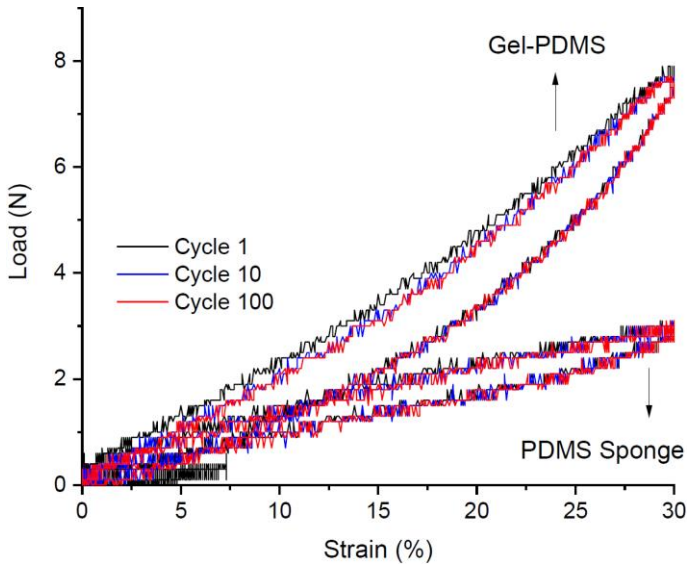


Figure S 11. Load-strain curves for cyclic compression testing of the gel-PDMS and PDMS sponge (dry-PDMS condition) materials to a strain limit of 30% with no pause phase at a strain rate of 0.83 s^{-1}. Graphs for cycles 1, 10 and 100 only are presented for clarity since there was no noticeable difference between cycles 2 to 100. The 2nd to 100th cycles consecutively started from the tare load immediately following an unloading phase to tare load with no waiting time.

Compressive moduli values for human, swine and bovine cartilages

Table S 2 shows the compressive moduli values reported in literature for three different source of cartilage. It is clear that the compressive equilibrium value observed for gel-PDMS is similar to the values found for human cartilage in similar testing parameters.

Table S 2. Comparison between compressive moduli values reported for human (5), swine (1) and bovine (1) cartilages and the compressive modulus found in this study for the gel-PDMS material.

Cartilage source	Testing configuration	E/H modulus (MPa)			Strain limit-Strain rate(or compression speed)	References
Swine knee	Unconfined	Mean: 0.389 (0.546±0.158 and 0.231±0.024 for 6 and 10 mm diameter samples respectively			Up to 20%-1um/s	#37 in the main paper (Machado, J.; Viriato, N.; Marta, M.; Vaz, M. J. R.; Medicine, O. Experimental Characterization of the Mechanical Properties of Knee Articular Cartilages in Compression: First Approach with Swine Tissues. 2017, 2 (4), 1-4.)
Human Glenoid and Humeral Head	Confined	0.351-0.543 (at 16% strain)			16% and 50%- $0.1x10^{-3}$-$0.2x10^{-3}$ s^{-1}	#60 in the main paper (Loy, B. N.; Zimel, M.; Gowda, A. L.; Tooley, T. R.; Maerz, T.; Bicos, J.; Guettler, J. J. O. j. o. s. m. A Biomechanical and Structural Comparison of Articular Cartilage and Subchondral Bone of the Glenoid and Humeral Head. 2018, 6 (7), 2325967118785854.)
Human patellae	Unconfined	Approximated to be 0.3-0.8			Total strain limit of 15% (including 5% pre-strain)- $0.28x10^{-3}$-$0.45x10^{-3}$ s^{-1}	#39 in the main paper (Julkunen, P.; Wilson, W.; Jurvelin, J. S.; Rieppo, J.; Qu, C.-J.; Lammi, M. J.; Korhonen, R. K. J. J. o. b. Stress–Relaxation of Human Patellar Articular Cartilage in Unconfined Compression: Prediction of Mechanical Response by Tissue Composition and Structure. 2008, 41 (9), 1978-1986.)
Human knee articular cartilage	Unconfined (E) and confined (H)	Unconfined :0.581 ± 0.168 Confined: 0.845± 0.383			20%- 10^{-3} s^{-1}	#35 in the main paper (Jurvelin, J.; Buschmann, M.; Hunziker, E. J. P. o. t. I. o. M. E., Part H: Journal of Engineering in Medicine. Mechanical Anisotropy of the Human Knee Articular Cartilage in Compression. 2003, 217 (3), 215-219.)
Bovine humeral, patellar and femoral cartilage	Unconfined and confined	Humeral	Patellar	Femoral	20% - $0.7x10^{-3}$ s^{-1}	#36 in the main paper (Korhonen, R.; Laasanen, M.; Töyräs, J.; Rieppo, J.; Hirvonen, J.; Helminen, H.; Jurvelin, J. J. J. o. b. Comparison of the Equilibrium Response of Articular Cartilage in Unconfined Compression, Confined Compression and Indentation. 2002, 35 (7), 903-909.)
		E:0.80 ±0.33	E:0.57 ±0.17	E:0.31 ±0.18		
		H:0.87 ±0.36	H:0.66 ±0.19	H:0.38 ±0.19		
Human femoral head	Unconfined-peak load	1.60-2.47			Up to load equivalent of 0.1MPa (~8%)-0.0167 s^{-1}	Burgin et la. "The mechanical and material properties of elderly human articular cartilage subject to impact and slow loading, 2013"

Human femur, tibia and patella knee	Unconfined and confined	Unconfined: equilibrium modulus: 0.22-0.557, instantaneous modulus 0.85-5.24 MPa	15%- 0.2 s^{-1}	A.Chokhandre et al. "A comprehensive testing protocol for macro-scale mechanical characterization of knee articular cartilage with documented experimental repeatability, 2020"
Gel-PDMS composite	Unconfined-both sides permeable	Equilibrium: 0.452 Peak: 0.910	10%-30%-0.83 s^{-1}	This work

Reference:

(1) Minns, R.; Steven, F. The collagen fibril organization in human articular cartilage. *Journal of anatomy* **1977,** *123* (Pt 2), 437.

(2) Lim, E.-H.; Sardinha, J. P.; Myers, S. J. A. o. p. s. Nanotechnology biomimetic cartilage regenerative scaffolds. **2014,** *41* (3), 231.